Engineered Science
DOI: https://dx.doi.org/10.30919/es8d800

Direct 3D Printing of Piezoelectrets: Process Feasibility, Prototypes Fabrication and Device Performance

Xiaolin Wang,[1, 2] Zhe Liu,[1, 2] Hui Wang[1, 2] and Changchun Zeng[1, 2,*]

Abstract

Piezoelectrets (or piezoelectric polymer foams) are porous piezoelectric materials with a wide range of applications particularly sensing. They have been successfully fabricated different techniques such as foaming, and fusion assembled of preformed structures. These fabrication techniques face several challenge issues such as limited structure design space and structural uniformity control. In this study we demonstrated direct 3D printing of piezoelectrets with designed pore structure using fusion deposition modeling (FDM). The feasible printing conditions was first explored using a response surface methodology to address challenges unique to piezoelectret structures. Subsequently, two types of prototypes were successfully printed with a maximum piezoelectric coefficient d_{33} ~1000 pC/N achieved. By varying the structure design, performance of the piezoelectrets can be customized over a broad range that was not attainable via other technologies. We finally demonstrated the sensing application of the printed piezoelectret sensors.

Keywords: 3D printing; Piezoelectret; Polypropylene, Piezoelectric activity, Sensors.
Received: 24 October 2022; Revised: 14 November 2022; Accepted: 29 November 2022.
Article type: Research article.

1. Introduction

Piezoelectrets are space charged porous polymers with high piezoelectricity.[1,2] The charged pores deform under external pressure, which result in the change of the charge density inside the pores and electrical signals. A great deal of polymer materials have been studied and developed as the piezoelectrets, including fluorinated ethylene propylene (FEP),[3-6] Polypropylene (PP),[7-11] Cyclic olefin copolymer (COC)[12,13] and fluorocarbon polymers.[3,14-21] Some devices based on the piezoelectrets such as microphones,[22] ultrasonic transducers,[23,24] piezoelectret accelerometers[25] and energy harvesters[26-28] have been demonstrated. Among all the piezoelectrets, PP remains the most commonly used one due to its flexibility and processibility.

Piezoelectric coefficient d_{33} is one of the most commonly used parameters in measuring the sensing performance of the piezoelectric material and it was defined by Equation (1):

$$d_{33} = \frac{\Delta Q}{\Delta F} = k\frac{\sigma}{Y} \quad (1)$$

Where ΔQ is the charge variation, ΔF is the force applied, k is a constant related to the material properties, Y is the Young's modulus of the piezoelectret and σ is the charge density.

The modulus of a porous material Y_p is dependent on the porosity and the aspect ratio of the pores following Equation (2):[29]

$$Y_P = Y_S \phi^2 / A \quad (2)$$

where Y_S is the modulus of the solid material, ϕ is the porosity and A is the aspect ratio. Both of the values are highly determined by the pore geometry. As shown in Fig. 1.

The pore aspect ratio A can be calculated by Equation (3):

$$A = \frac{d}{h} \quad (3)$$

where, d is the unit cell length and h is the unit cell height. For high piezoelectric sensitivity, a porous material with high porosity and high pore aspect ratio would be highly desired. In addition, there is also an optimal range of the pore height, which has significantly influence on the charging process and the charge densities σ. In general, h should be below a few hundred micrometers to ensure a high charging capability.[30] Therefore, highly sensitive piezoelectrets demand a

[1] *Department of Industrial and Manufacturing, FAMU-FSU College of Engineering.*
[2] *High-Performance Materials Institute, Florida State University, Tallahassee, FL 32310, USA.*
[*] *E-mail:* zeng@eng.famu.fsu.edu (C. Zeng)

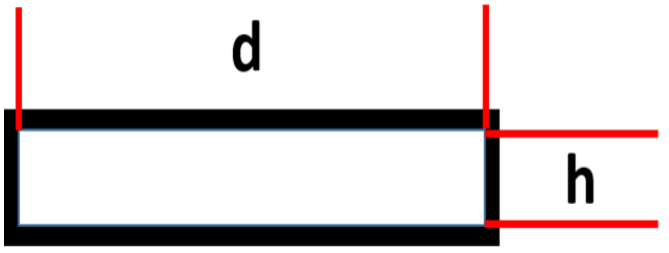

Fig. 1 Illustration of the pore aspect ratio.

manufacturing process that can produce porous structures with high anisotropy and high porosity and optimal pore height. Furthermore, a process capable of producing porous structures with well-controlled structure parameters would represent a major progress in realizing precise control of the porous structure-piezoelectric property relationship. The two prevailing methods employed in the piezoelectret fabrication cannot meet these requirements. The first method is a three-step process involving 1) directly foaming, 2) follow-up bubble expansion and 3) shaping.[9,31,32] The first step generates initial foams with limited porosity. The porosity is increased in the expansion step, resulting in a foam with isotropic pores. Shaping step is the taken to increase the anisotropy. For instance, the PP film with micro-pores was first obtained by the co-extrusion of the PP and $CaCO_3$. A lens-shape pore structure with large aspect ratio was obtained through uniaxial stretching during the foaming process. Then the PP film was placed in a high-pressure vessel and the pores are inflated when the high pressure was rapidly released to further control the pore height. Piezoelectrets with a piezoelectric coefficient around 300 pC/N can be obtained.[32] This method is unable to produce precisely controlled pore structure, as the direct foaming is a highly stochastic process, leading to foams with a broad range of pore size distribution with limited reproducibility. To address this intrinsic inability, a new method was developed which utilized the fusion of multi-layers films with pre-formed cavity. A designed pattern was first generated on a single layer by various techniques such as laser cutting,[12] molding,[3] UV-lithography.[33] The individual layers were subsequently fused together. Porosity and pore dimension can be adjusted by the pattern design and lay-up pattern. For instance, Zhang *et al.*[3] employed molding for the FEP pattern design and the as-prepared FEP films are bonded together via hot pressing. This resulted in better pore distribution control than direct foaming. However, bonding of the multi-layers relies on partial melting of the polymers, which inevitably also resulted in the deformation and sometimes collapsing of the pore structure. To overcome this, Li *et al.*[12] developed an supercritical fluid assisted assembly process and achieved fusion of multi-layer structure at temperature far below the softening/melting temperature of the polymer and largely preserved the designed pore structure. A piezoelectric coefficient of as high as 1500 pC/N was reported. Nevertheless, the bonding strength achieved was moderate, which may affect the long-term stability of structure. The fusion process also suffers from constrained designability as the structures amenable to fusion with good stability and structural fidelity are limited. New techniques which could fully realize the design potential for piezoelectrets fabrication are in highly needed.

As an emerging versatile and low-cost manufacturing technology that is highly customizable, 3D printing is ideally suited to address the shortcomings of current piezoelectrets fabrication methods to fully realize the design potential, *e.g.*, properties by design. A great deal of research has been reported in 3D printing of medical devices,[34-37] structural materials,[38] as well as cellular polymer structures.[39,40] Comparing to these structures, the specific geometric requirements of piezoelectrets poses unique challenges on 3D printing. The high aspect ratio pore structure requires printing extensively overhang structure with large span and small layer height. A typical solution in the current 3D printing technology is to add supporting structures that needs to be removed later. For multi-layer porous structure involved in piezoelectrets printing, this is not feasible for piezoelectrets, as the close-pore structure would prohibit the removal of the entrapped support materials, resulting a solid instead of porous structure. Direct printing of extensive overhang structure with good structure fidelity is a critical challenge for piezoelectret printing. The challenging is further amplified by the small layer height requirement, because sagging of the layer may partially or completely block the pores and severely degrades the structure. The second challenge unique to the piezoelectret printing is the surface quality requirement. To render the structures piezoelectric, they must be charged under high electrical field, and the stored charge must have sufficient stability. Cracks in the printed structures reduces the electrical field strength and result in low or no charge. The render charges are also prone to migration through the cracks leading to reduced charge stability. Both have severe negative impact on the piezoelectric properties.

In this study we investigated direct 3D printing by fused deposition modeling (FDM) PP piezoelectret fabrication. Feasibility was first probed, and a response surface methodology was employed to investigate the feasible printing conditions. Two types of prototypes were successfully printed. A maximum d_{33} value of ~1000 pC/N was obtained from the directly printed PP piezoelectrets. Furthermore, performance

of the piezoelectrets can be highly customized by structure design that was not attainable via other technologies. For instance, by just adjust the pore geometry, sensors with varying sensitivity and sense range were successfully printed. We finally demonstrated the sensing application of the printed piezoelectret sensors.

2. Materials and methods

2.1 Piezoelectrets fabrication

2.1.1 Structure design

Leveraging the flexibility of 3D printing, two types of prototype structures, P1 and P2, were designed and printed for piezoelectrets. Both types of structures possess low compressive modulus, beneficial for piezoelectric activity. Their compressive moduli and unit cell geometry can be further tuned to tailor the mechanical and electromechanical properties. Prototype P1 is a non-overlap structure with 5 layers shown in Fig. 2(a). Li *et al.*[12] first demonstrated such a structure resulted in very low compressive modulus by inducing large bending deformation of the structure units.[12,41] This is illustrated in Fig. 2(b) schematically. Fig. 2(c) illustrates the design parameters of this type of structure, thickness of the solid layer (layer height) h_1, the porous layer thickness (pillar height) h_2, the pillar width w and the pillar spacing d. Figs. 2(d) and (e) show the structure and the mechanical deflection under pressure of prototype P2. It is a 3-layer structure, in which a square-shaped cavity containing middle layer was sandwiched between two solid layers. Three structure parameters, cavity length L, solid layer thickness h_1, and cavity depth h_2, were varied to control the modulus and charge densities of the overall structure (Fig. 2(f)).

2.1.2 3D printing of prototypes

Fused deposition modelling (FDM) was employed to 3D print both prototypes using polypropylene (PP) filament (purchased from Gimzo Dorks with d=2.85 mm). The 3D printer used was Lulzbot TAZ5 with 0.5 mm diameter nozzle. A feasibility study was first conducted by investigating the impacts of the printing conditions (printing temperature, printing speed, layer height and flow rate) on the printing quality. Flow rate is defined as the ratio of the amount of the filament actually extruded to the filament calculated needed to be extruded. The detailed processing conditions are summarized in Table 1.

Followed by the initial feasibility study, a Box-Behnken response surface method was employed to further explore and identify the feasible processing regions. They were used to print the designed structures and prototypes for further characterization.

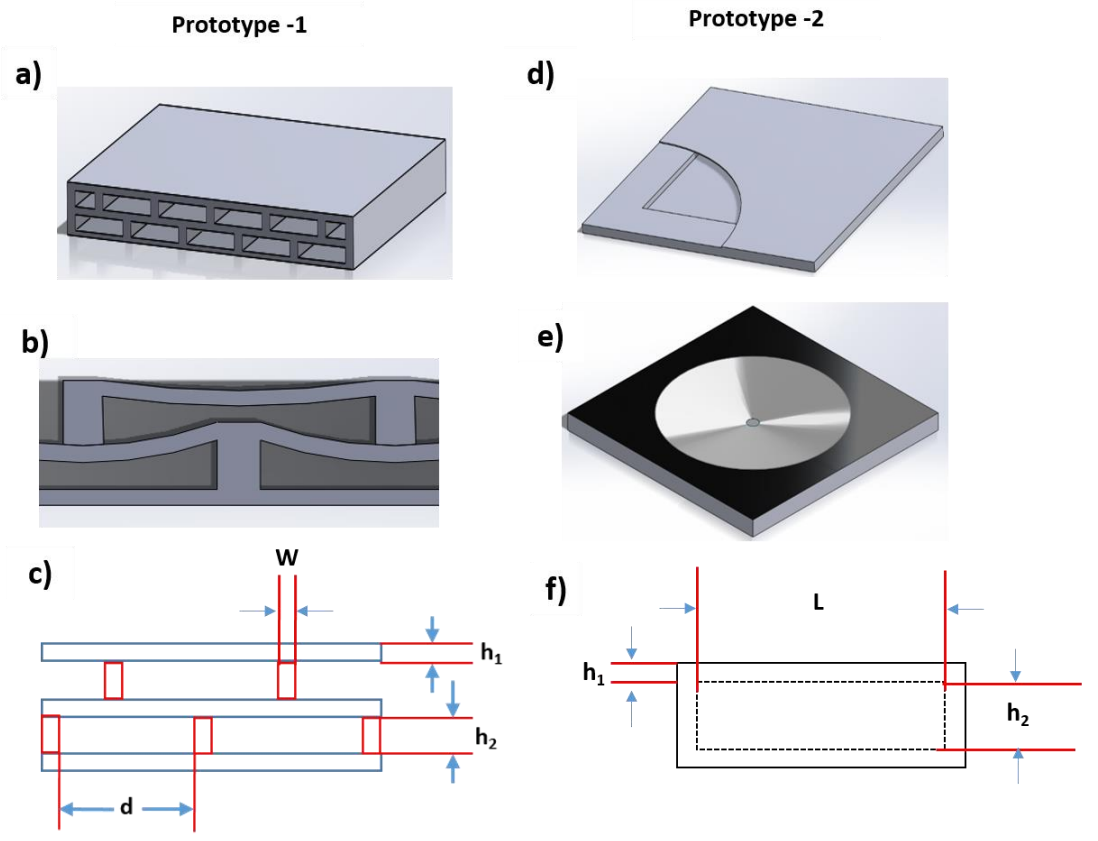

Fig. 2 Schematics of the designed overall structures for prototype-1(a) and prototype-2(d); illustration of the mechanical deformation for a unit cell under equally distributed force F for prototype-1 (b) and prototype-2 (e); illustration of the structure parameters to control the mechanical deformation of protype-1 (c) and prototype-2 (f).

Table 1. Printing parameters investigated for the feasibility study.

Parameter / Level	Speed (mm/s)	Flow rate (%)	Layer height (mm)	Temperature (°C)
Low	10	100	0.1	190
Medium	30	110	0.2	210
High	50	120	0.3	230

2.1.3 Charging of prototypes

The as-printed samples were coated with a 1 × 1 cm^2 square copper electrode on both the surface and bottom layer. The samples were charged in room temperature by contact charging using a precision high voltage power supply (PNC10000-6ump, Heinzinger electronic Gmbh). The voltage employed was 8 kv and the charging process lasts for 10s. Then the charged samples were placed between aluminum foil for 24 h to stabilize the accumulated charges.

2.2 Piezoelectrets characterization

2.2.1 Characterization of printing quality

Two qualities critical to the piezoelectret performance were characterized: surface quality and fidelity of the overhang structure. The printing surface quality was characterized by the crack area/surface ratio (CSR). CSR is defined as the ratio of the crack surface area to the total surface area. The charges in the piezoelectric foams are stored in the cells created by each layer. A dense film is required to retain the charges and any crack would result in charge leakage. Therefore, the crack area in the samples is the most critical factor which need to be addressed. A photograph of the top surface of each printed sample was taken. The image was imported into ImageJ and converted into binary image. Cracked areas (gap regions between printed polymers) were identified and the size of each crack measured. The ratio of the total cracked area over the size of the top surface, crack surface ratio (CSR), was used as an index for surface quality. A lower ratio would indicate a printed surface with less discontinuity and better printing quality. A value of 0 would mean a printed surface devoid of separation of polymer, and an entirely continuous surface. Only the samples with CSR value of zero will be used to further characterization.

The degree of deformation of the structure was observed to evaluate the quality of the printed overhang structure. The as printed samples were first cut through using a laser cutting machine. The exposed cross-section was observed by optical microscopy. A dino-light camera was used to take the images of the sideview of the samples at 50x magnification.

2.2.2 Electromechanical property characterization

(1) Charge build-up characterization

Hysteresis loop measurements were performed to study the piezoelectrets charging process using Precision Premier II (Radiant technologies, Inc.). Charging voltages from 1kv to 9kv with bi-polar mode (TREK Model 609B) were applied onto the printed samples. The remnant polarization strength P_r was then recorded. For each voltage, 5 tests were performed to calculate the average P_r.

(2) Piezoelectric property characterization

The piezoelectric coefficient d_{33} were measured by the quasi-static method using a Keithley electrometer (6517A, Keithley Instruments, Inc.). The d_{33} was calculated by the well-known equation: d_{33}=Q/F, in which Q is the induced charge variation and the F is the applied force. A pre-load of 0.2N was applied on the top surface to minimize the air gap effect in all the measurements. A set of pre-calibrated loads varies from 0.49N to 4.9N were first applied onto the sample to a 1 × 1 cm^2 square electrode, then removed. The induced charge Q was then recorded and integrated in 10s. Values averaged from 5 separate measurements were reported.

(3) Mechanical displacement simulation

COMSOL Multiphysics was employed to simulate the deformation of the printed piezoelectrets. The geometries of the two prototypes were shown in Fig. 2. Finite element analysis (FEM) with the compression loading conditions were performed. During the simulation, a fine mesh was employed and the force was considered to be equally applied on the top surface while the position of the bottom layer was fixed. The elastic modulus of PP employed is 1800Mpa, the poison's ratio employed is 0.43 and the material density used is 930 g/cm^3. The material was considered to be total linear elastic.

2.3 Piezoelectret sensor device performance

Pressure sensing system was designed and fabricated to illustrate the pressure sensing capability of the piezoelectrets. A charge amplifier (TLV 2774, Texas Instrument) was used to convert the high-impedance signal to low-impedance signal for better measurement. The conversion circuit was demonstrated in Fig. 3. The resistor used was 10 kΩ and the capacitor used was 100pf. The power supply was set to 5 kv and the bias voltage was set to 2.5kv. Arduino nano circuit

board was employed as the data acquisition system. A set of loads from 20g to 200g were applied to the piezoelectric sensor and a real-time pressure-voltage correlation data was restored.

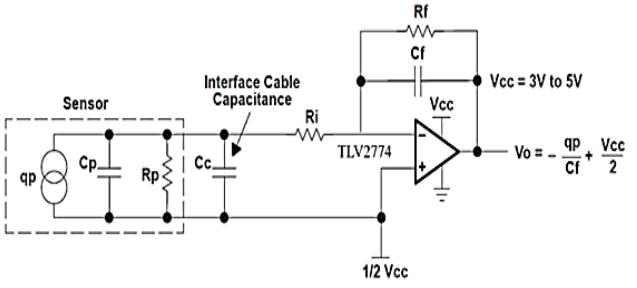

Fig. 3 Charge mode amplifier circuit for piezoelectric polymer foams.

3. Results and discussion

3.1 Feasibility studies of direct 3D printing of piezoelectrets

3.1.1 Feasibility study of printing surface with suitable surface quality

The effects of printing conditions on the printed surface quality were investigated. Fig. 4 shows photos of representative printed samples with high, low and zero CSR. Detailed printing conditions and additional photos of samples can be found in Fig. S1 in supporting information. It should be emphasized that only samples with 0 CSR were suitable for piezoelectret applications.

As shown in Fig. S1. The printing quality was only marginally affected by temperature, while printing speed, filament flow rate, and layer height all have significant influence. A large number of cracks and defects were observed in samples printed at high speed (50 mm/s). The printing quality was significantly improved by reducing the printing speed to around 10 mm/s. Layer height plays the most significant role in the printing quality. Printing a surface with layer height equals to 0.1 mm was not feasible because of the frequent and extensive filament breakage. For samples printed at 0.2 mm layer height, while the filament did not break, there were still many defects on the surface which rendered charging impossible. Zero CSR was achieved when the layer height increased to 0.3 mm. Regarding to the flow rate, it can be clearly seen that the filament undergoes an under-extrusion when the flow rate is 100% and 110%. To obtain a dense film, a flow rate of at least 120% was required. Fig. 5 summarized the impacts of different printing conditions, *e.g.*, temperature, printing speed, layer height and flow rate, on the printing qualities (CSR).

These results can be explained by the extrusion principles. As shown in Fig. 6(a), the filament was first pushed by the tooth shaft and melt by the heat chamber. The molten polymer was then pushed out from the nozzle and deposited onto the printing bed layer by layer. In the heat chamber, the filament was not melted instantaneously. Instead, there is always a melting front in the chamber which was mainly affected by the temperature and printing speed. As shown in Fig. 6(a), there are three pressure drop zones in the printing process, the entrance zone, the convergence zone and the capillary zone. Oswald-dewaele model was employed to assess the pressure drop of the three zones.[42] The pressure drop of the three zones were calculated from Equations (4)-(7).

Entrance zone:

$$\Delta P_1 = 2(L_1 - L_m)\left(\frac{V_1}{\varphi}\right)^{1/m}\left(\frac{m+3}{\left(\frac{D}{2}\right)^{m+1}}\right)^{1/m} gH(T) \quad (4)$$

Convergence zone:

$$\Delta P_2 = \left(\frac{2m}{3\tan\left(\alpha/2\right)}\right)\left(\frac{1}{d^{\frac{3}{m}}} - \frac{1}{D^{\frac{3}{m}}}\right)\left(\left(\frac{D}{2}\right)^2 (m+3)\, g 2^{m+3}\right)^{1/m} gH(T) \quad (5)$$

Capillary zone:

$$\Delta P_3 = 2L_2\left(\frac{v_1}{\varphi}\right)^{1/m}\left(\frac{(m+3)\left(\frac{D}{2}\right)^2}{\left(\frac{d}{2}\right)^{m+3}}\right)^{\frac{1}{m}} gH(T) \quad (6)$$

$$H(T) = exp\left[E_\alpha\left(\frac{1}{T} - \frac{1}{T_\alpha}\right)\right] \quad (7)$$

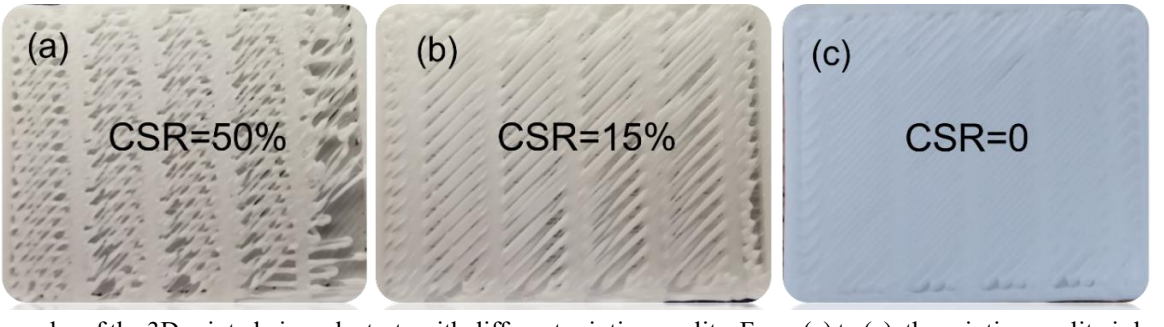

Fig. 4 Photography of the 3D printed piezoelectrets with different printing quality. From (a) to (c), the printing quality is bad, medium, and good, respectively.

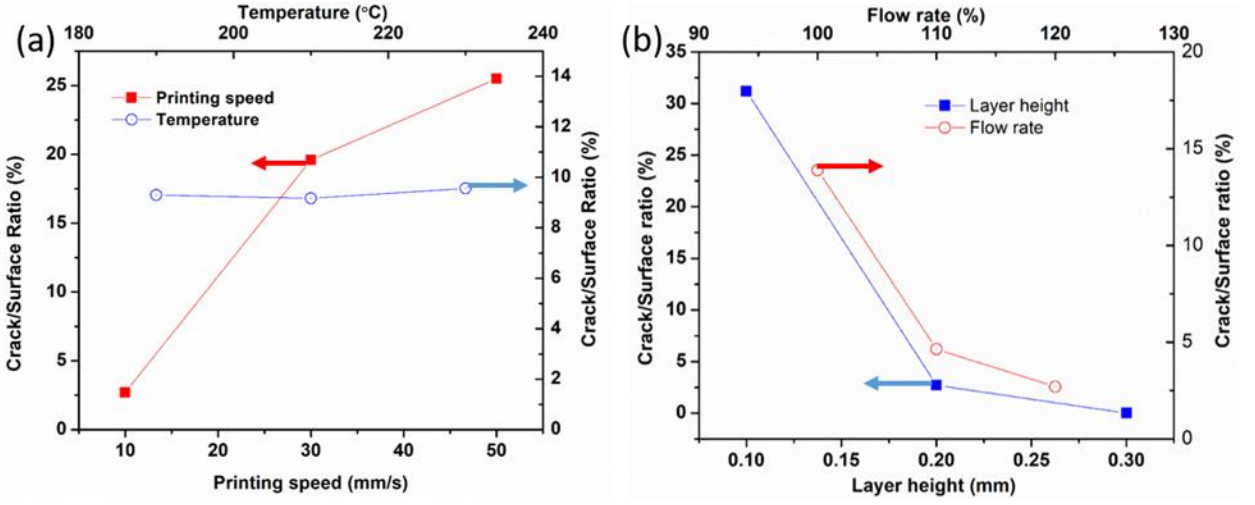

Fig. 5 Illustration of the impact of printing conditions on the surface quality. (a), the impact of temperature (blue) and the printing speed(red); (b) the impact of layer height (blue) and flow rate (red). The default printing parameters are 190℃, 30mm/s, 0.2mm layer height and 120% flow rate.

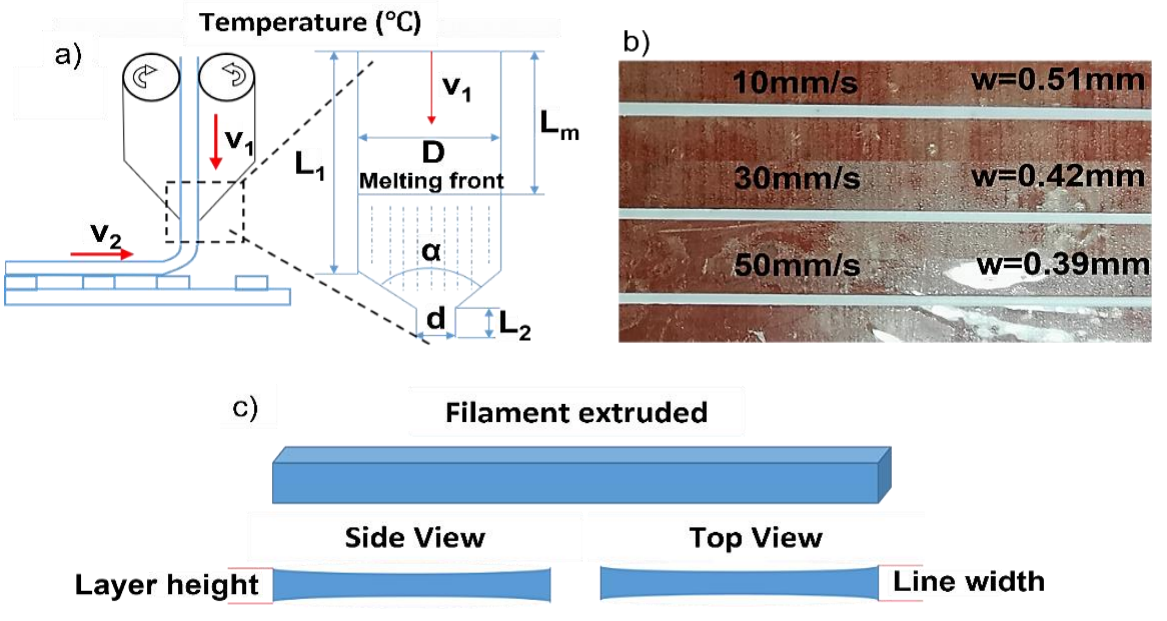

Fig. 6 (a) Illustration of the extrusion principle in the printing process; (b) photograph of the width of the filament printed with different printing speed; (c) illustration of the side view and top view of the filament printed.

Total pressure drop is[42]

$$\Delta P = \Delta P_1 + \Delta P_2 + \Delta P_3 \quad (8)$$

where m and φ are the flow exponent and the material fluidity, respectively; it should be noted the fluidity is the inverse of the viscosity by definition, L_1, L_2, D, d, and α are the geometry parameters of the liquefier which are well shown in Fig. 6(a). L_m is the length of the unmelt filament inside the chamber. E_α is the activation energy and H(T) is given by the Arrhenius law which T_α is the temperature where H(T) is 1. The melt front line is proportional to the fed in speed v_1.

Based on Equations (4)-(8), the pressure drop was impacted by the material property, nozzle geometry, temperature and the printing speed. For a given 3D printer and material, the factors adjustable are the temperature and the printing speed. Increase of the printing speed will generate huge back pressure which cause the amount of the filament fed in per step by the extruded stepper to reduce. As at high back pressure, each tooth compresses and skates over the surface of the filament for longer before it manages to bite. This phenomenon is called non-linear extrusion which the increase of the fed in speed cannot match up with the increase of the printing speed.

If we ignore the molten compression effect, the volume of the filament fed in should be the same with the volume of the filament that pushed out from the nozzle. Considering the cross-section of the printed fiber is rectangular with a line

width w and height h. Then we get Equation (9) (see supporting information for details on the derivation),

$$v = \frac{\pi D^2 v_1 t}{4} = whV_2 t \quad (9)$$

where V is the volume extruded in unit time, v_1 is the fed in speed, v_2 is the printing speed, t the unit time, D is the diameter of the heat chamber, h is the layer height and w is the line width of the printed filament. As the printing speed and layer height are fixed by the software and the nozzle geometry won't change during the printing, the lower fed in speed is compensated by the thinner line width. Thus, the line width for each fiber printed decreases. The higher the printing speed, the thinner the printed fiber. The single fibers printed in different speed are shown in Fig. 6(b). Therefore, the under-extrusion occurred when the flow rate is 100% or 110%. In addition, the overhang structure poses more challenges as the printed fibers would shrink in both the horizontal and the vertical direction because of the lack of support. As shown in Fig. 6(c), the fiber thickness decreases when stretched. When the layer height is too low (*e.g.*, 0.1mm), the line breaks during the printing which causes the overall printing process to fail.

In a typical 3D printing process, the samples are usually printed in multiple layers, the small gaps between the extruded filaments may be filled with the next layer, and the solid support from the previous layer will help alleviate this issue. Therefore, in a typical 3D printing the line breakage will not cause printing failure. However, 3D printing of piezoelectret requires printing a single layer of a very thin film. Defects in the single layer is fatal to store the accumulated charges. As shown in Fig. 5, either increase the layer height or increase the flow rate will help resolve the problem; however, the increased layer height will decrease the deformability and the increased flow rate will cause unexpected dimension accuracy problem as more materials are extruded. Therefore, our goal is to find feasible printing conditions that can achieve a structure with 1) zero CSR; 2) the small possible layer height; and 3) maintaining a flow rate below significant over-extrusion (below 120%) with a reasonable printing speed (>10mm/s). To find this processing region, a response surface method (RSM) was employed with three continual factors investigated: printing speed, layer height and flow rate. A Box-Behnken design was employed to minimize the number of needed experiments. The three factors were coded into 3 levels (-1, 0, 1) and a total number of 13 runs were performed. The feasible printing conditions which could fulfill all the three demands shown above could be found from the contour images.

The detailed RSM design and results were shown in Table 2 and the RSM produces the following relationship between the CSR with the flow rate, layer height and printing speed:

$$CSR = 2.28 - 1.22\,f - 10.321h + 0.00567\,v - 0.03f^2 + 12.53h^2 + 0.000035v^2 + 3.328\,fh + 0.00007fv - 0.02435hv \quad (10)$$

where f is the flow rate, v is the printing speed and h is the layer height.

Table 2. Design and results of printing parameters using response surface methodology.

Flow rate (coded value)	Layer height (mm) (coded value)	Printing speed(mm/s) (coded value)	Crack/Surface ratio (CSR)
100% (-1)	0.1(-1)	10mm/s(-1)	71.21%
		50mm/s(1)	81.20%
	0.3(1)	10mm/s(-1)	4.75%
		50mm/s(1)	8.61%
120% (1)	0.1(-1)	10mm/s(-1)	29.80%
		50mm/s(1)	53.20%
	0.3(1)	10mm/s(-1)	0.00%
		50mm/s(1)	0.51%
center (0) 110%	0.2(0)	30mm/s(0)	9.30%
100% (-1)	0.2(0)	30mm/s(0)	13.90%
120%(1)	0.2(0)	30mm/s(0)	6.80%
110%(0)	0.1(-1)	30mm/s(0)	49.13%
	0.3(1)	30mm/s(0)	2.68%
110%(0)	0.2(0)	10mm/s(-1)	4.64%
		50mm/s(1)	11.94%

To further explore the feasible processing region, the CSR contour images obtained from Equation 10 was shown in Fig. 7. For better illustration, the layer height was fixed in each contour image, *e.g.*, 0.1 mm (Fig. 7(a)), 0.2 mm (Fig. 7(b)) and 0.3 mm (Fig. 7(c)), respectively. In each case the feasible region ($CSR \leqslant 0$) is marked in black. As shown in Figs. 7(a) and (b), the feasible regions do not exist with layer height h equals to 0.1mm and 0.2mm. When the layer height increases to 0.3 mm, a small feasibility region appears (Fig. 7(c), circled top left corner) with a minimum flow rate of 118% and a maximum printing speed of 25mm/s.

Based on the RSM study, for the following prototypes printing we used a set of fixed printing conditions with a layer height of 0.3mm, flow rate of 120% and printing speed of 20 mm/s.

3.1.2 Feasibility study of printing the overhang structures

From the study above, we found the acceptable printing conditions to obtain a continuous film and the minimum layer height required is 0.3mm. However, the inevitable sagging is still a concern that may affect the piezoelectric performance. The sagging phenomenon was illustrated in Fig. 8(a). Sagging of the printed film would affect the actual pillar height in the piezoelectret and therefore the piezoelectric performance. To

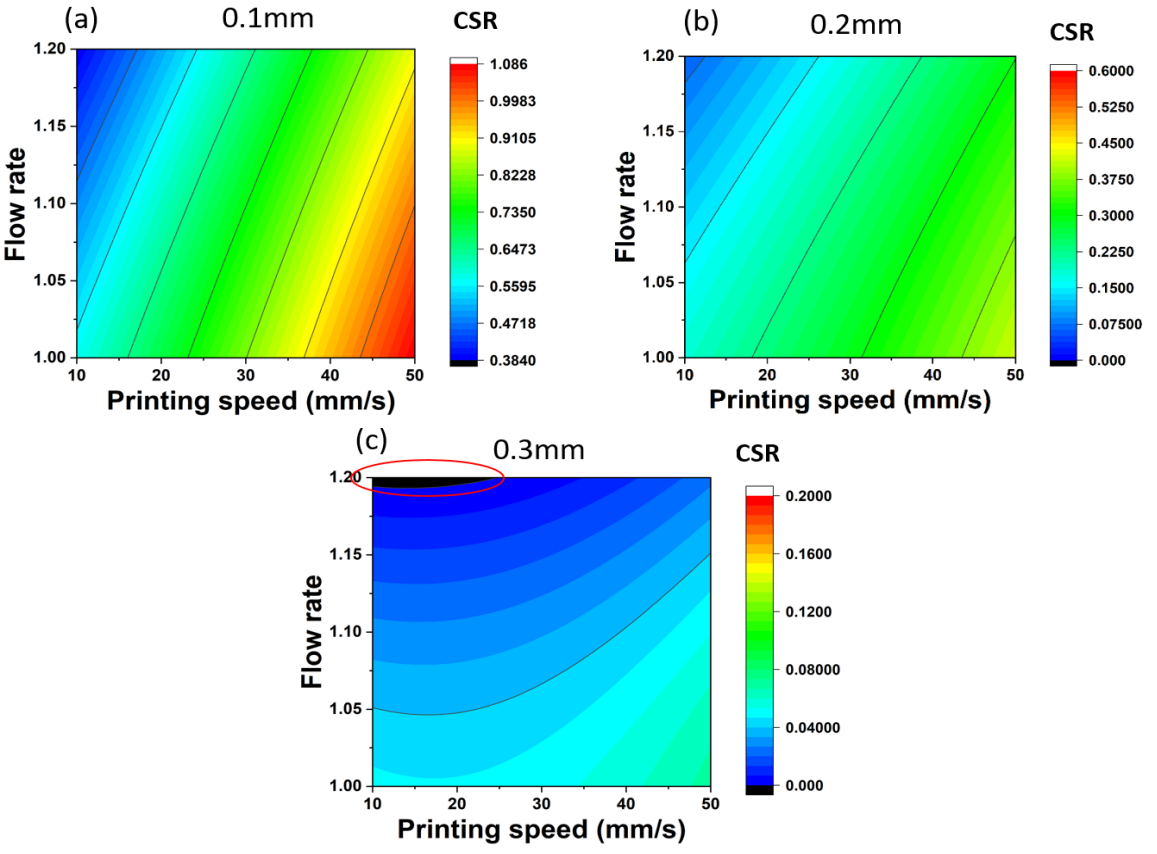

Fig. 7 Contour images of the CSR vs. flow rate and printing speed with different layer heights: h_1= 0.1mm, 0.2mm and 0.3mm for (a), (b) and (c), respectively.

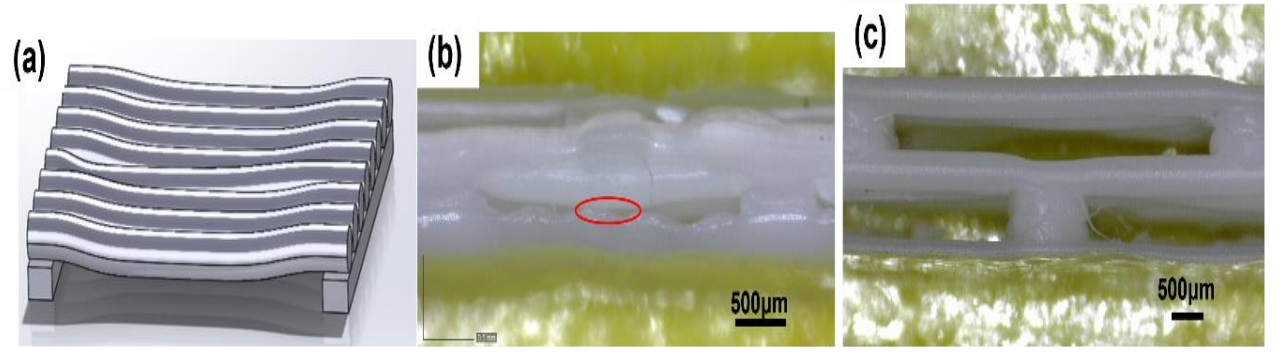

Fig. 8 Illustration of the sagging phenomenon in the overhang structure printing (a); optical microscopy of the side view of the samples printed with pillar height h_2=0.3mm (b) and 0.6mm (c), respectively.

achieve best piezoelectric performance, several hundred micrometers of pillar height are in need. Therefore, two pillar heights: 0.3mm and 0.6mm were selected to study the printing quality of the overhang structures.

The side view of the samples with different pillar height is shown in Figs. 8(b) and (c). With a pillar height design value of 0.3mm, the actual height varied greatly along the printing direction. In some region, the upper layer even contacts with the bottom layer. The severe sagging problem could be expected as 0.3mm is too small that a minute vibration of the printer may cause the upper layer contact with the bottom layer and the overall printing process fails. The sagging problem was largely resolved by increasing the pillar height to 0.6 mm. Sample with designed pillar height around 0.6mm were printed with good dimension control (Fig. 8(c)). Therefore, a pillar height of 0.6mm was used in the printing of piezoelectrets for the remainder of the study.

3.2. Piezoelectrets prototypes printing

3.2.1 Prototype 1 (P1)

Guided by the feasibility study, appropriate processing parameters were selected to successfully print a series of

prototype-1 structures. These prototypes have the same pillar height h_2 of 0.6mm and pillar width w of 1mm, while the pillar spacing varies from 3mm to 6mm (Table 3).

Table 3. Prototype 1 with different pillar spacing d.

Prototype 1 (P1)	Pillar space d (mm)
P1-1	3
P1-2	4
P1-3	5
P1-4	6

The printed samples were charged using contact charging, and the charge densities were measured. Fig. 9(a) shows the results. The data form a single master curve. This is understandable as the charge build is primarily dictated by the electrical field strength. Since the samples all have the same layer height, they would experience identical field strength under the same electrical voltage. The charge density remains very low until the charging voltage reaches 7kv and then rapidly increase from 7kv to 9kv. This indicates that the breakdown voltage for the samples is around 7kv. Piezoelectrets were prepared by charging the printed samples at 8kv, and their piezoelectric coefficients d_{33} were measured. Fig. 9(b) shows the results. All samples exhibited moderate piezoelectric activity. d_{33} decreases slightly with increasing pressure. Higher d_{33} was observed for piezoelectrets with large pillar space, resulting from the larger deformation of the structure. To illustrate this, COMSOL simulation was conducted, and the maximum displacement was calculated. Fig. 9(c) shows the results, the displacement increases with increasing layer space. Such a larger deformation would imply a lower effective modulus, leading to a higher piezoelectric sensitivity. To our knowledge, this was the first time piezoelectrets were successfully fabricated by direct 3D printing.

3.2.2 Prototype-2 (P2)

Prototype-2 is a three-layer structure with the cavity directly generated between the top and bottom layer. The key parameter in this structure is the cavity length L and the cavity depth h_2. For the printed prototype piezoelectrets, the cavity depth was 0.6mm and the cavity length varied from 12 to 18mm. The detailed cavity length L were shown in Table 4.

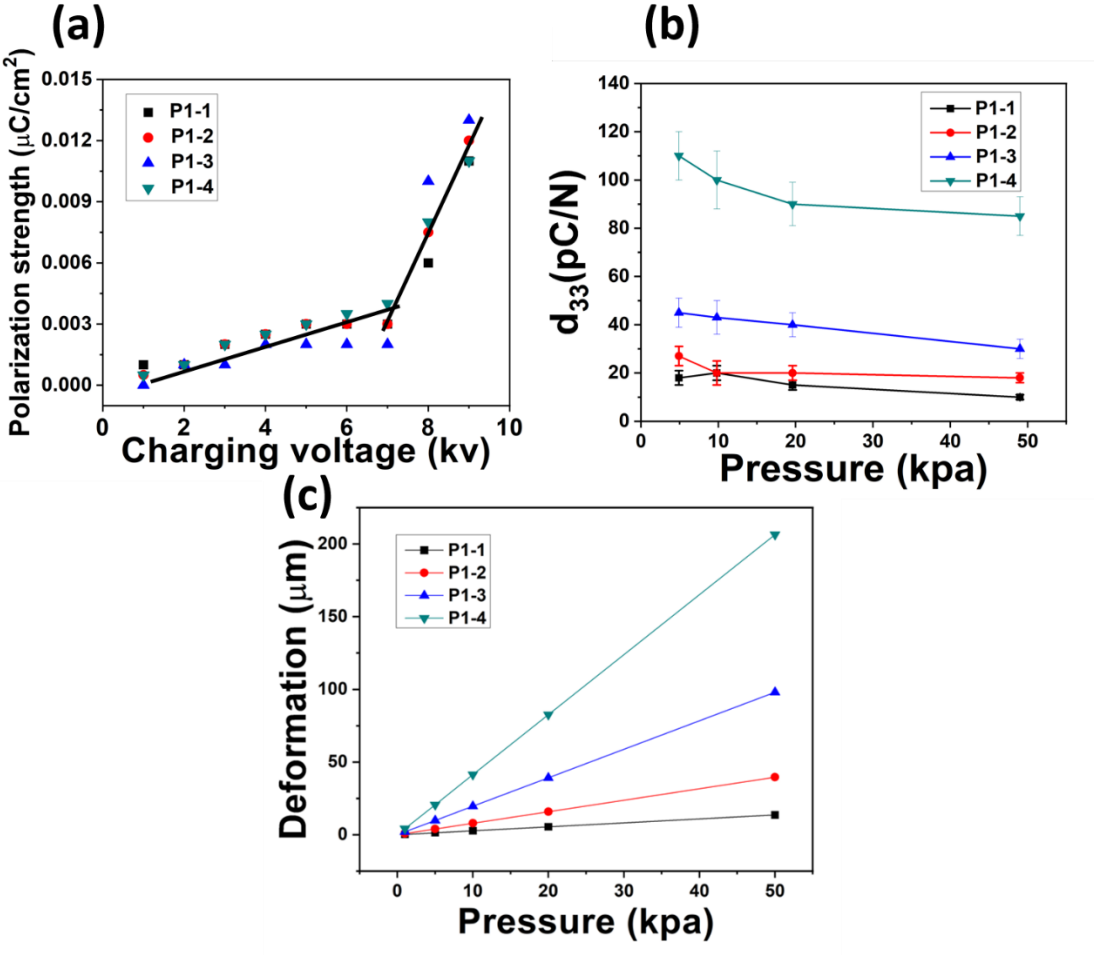

Fig. 9 (a) the remnant polarization strength vs. charging voltage to show the breakdown voltage of the P1 structure; (b) the d33 results of the P1 structures and (c), the COMSOL simulation of the maximum displacement for the structures with different pillar space d.

Table 4. Protype-2 with different hole length L.

Prototype 2 (P2)	Hole length L (mm)
P2-1	12
P2-2	15
P2-3	18

A hysteresis loop test has also been performed for the three types of the samples to obtain the charge buildup characteristics and Fig. 10(a) shows the results. Again, a single master curves was observed. The dielectric breakdown occurred at around 6kv, lower than that observed for prototype-1 piezoelectrets. The piezoelectric d_{33} for different piezoelectrets of P2 were measured and Fig. 10(b) shows the results. All piezoelectrets showed good piezoelectric activity that is higher than that achieved by prototype 1 piezoelectrets reported earlier. The piezoelectret with the largest length (L=18 mm) showed the highest piezoelectric d_{33}, over 1000 pC/N at low pressure. The piezoelectric activity decreased with increasing pressure, and the decrease in more significant in piezoelectrets with the largest hole length L=18mm. Nevertheless, all piezoelectrets maintained substantial d_{33} at high pressure. COMSOL simulation was also conducted on the Prototype 2 and the maximum displacement was calculated. Fig. 10(c) shows the results, the displacement increases with increasing hole length L and the maximum displacement is much higher than that of the prototype-1, indicating the larger d_{33}.

4. Pressure sensing by prototype piezoelectrets

Two types of force/pressure sensors were successfully fabricated by the two structures P1-4 and P2-3. The sensor system was shown in Fig. S2. A set of load varies from 20g to 200g were loaded onto the sensor and the voltage outputs were measured and recorded. Figs. 11(a) and (b) show the sensors response. An increase of the signal output with the increase of the load could be observed for sensor P1-4. The signal output of the P2-3 sensor also increases with the increase of the load in small force range (<100g) but plateaus under higher force. To better illustrate the differences of the two sensors, the response of the two sensors were plotted in Fig. 11(c). P1-4 sensor almost shows a linear output through the entire pressure range. P2-3 sensor also shows linear output in low pressure range with a higher sensitivity. The sensor performances are in consistent with the d_{33} testing results in the previous section. However, with the further increase in pressure, the signal begins to be saturated because the maximum deformation of the structure has been reached.

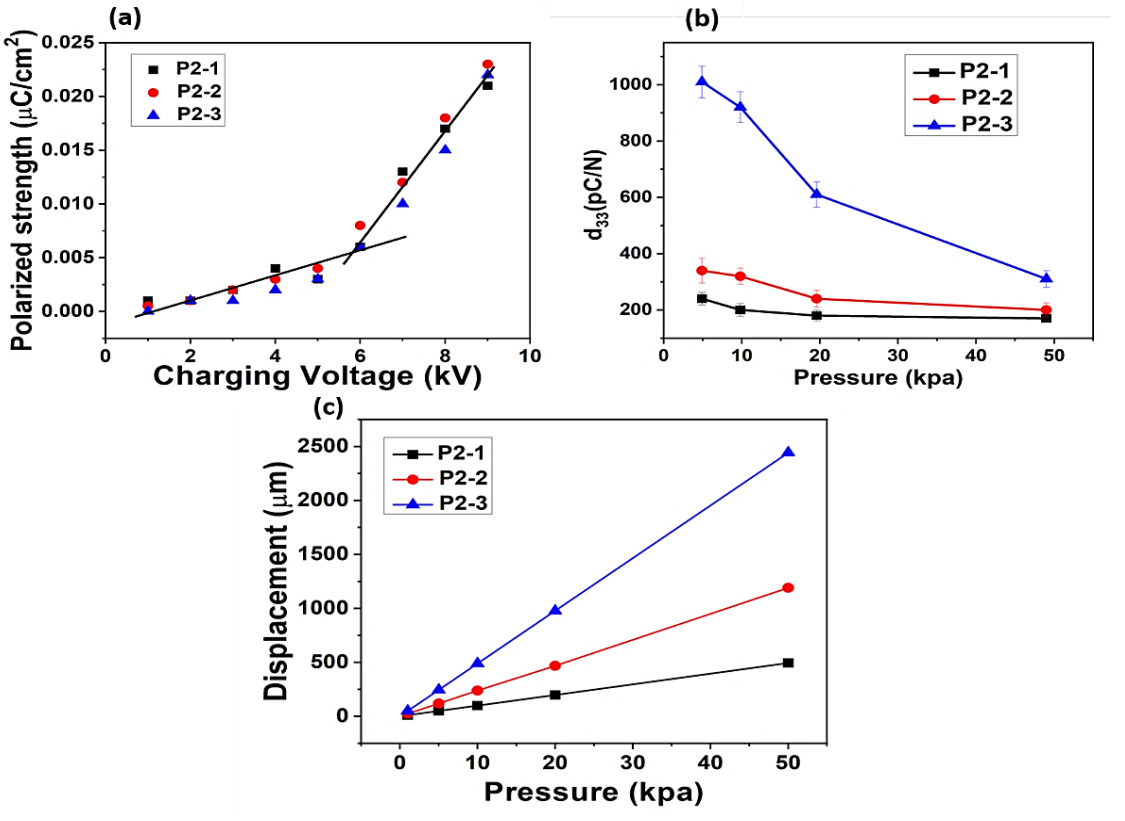

Fig. 10 (a) the remnant polarization strength vs. charging voltage to show the breakdown voltage of the P2 structure; (b) the d_{33} results of the P2 structures and (c), the COMSOL simulation of the maximum displacement for the structures with different hole length L.

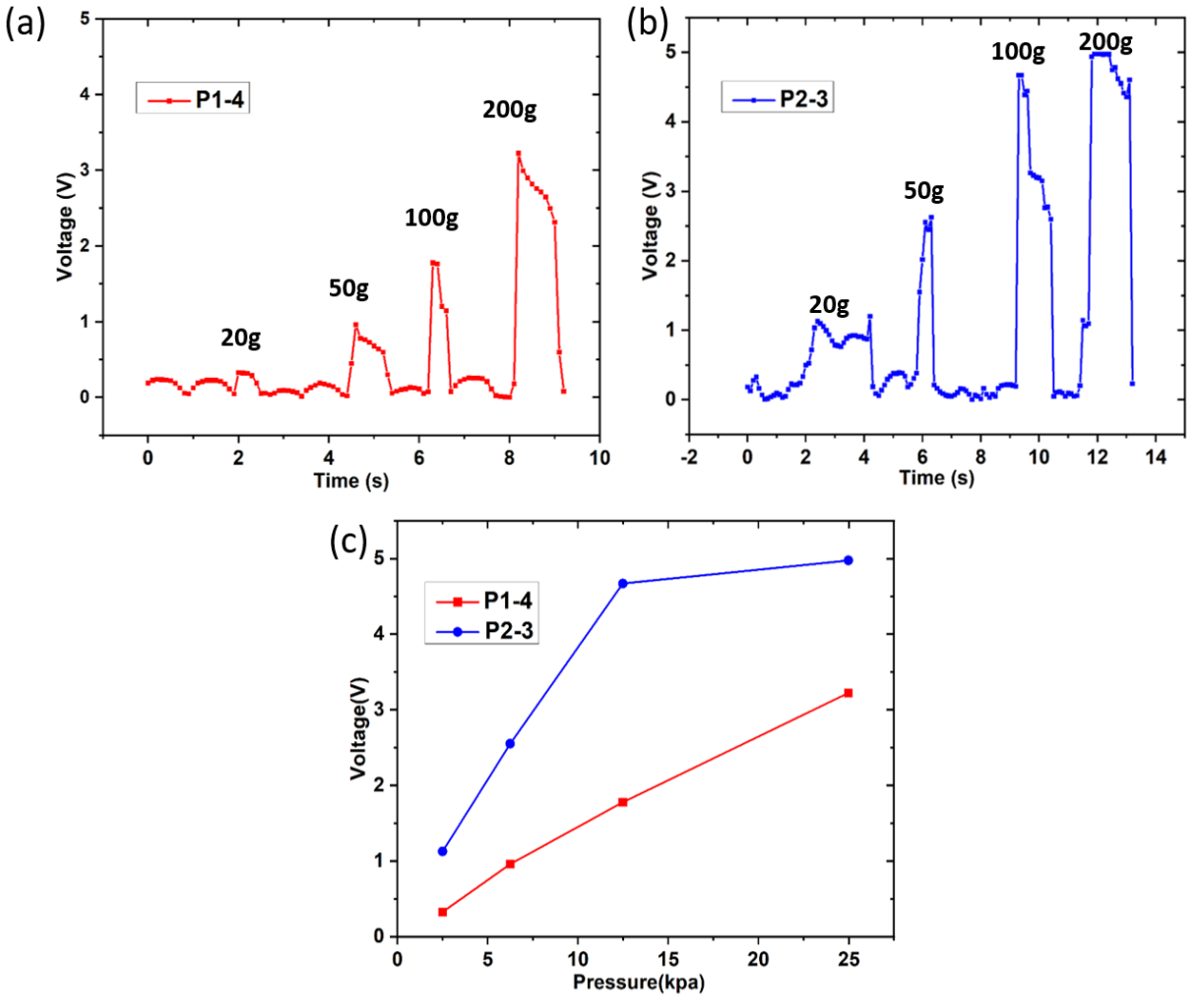

Fig. 11 Sensor performance of the piezoelectrets: real-time response of the P1 sensor (a) the P2 sensor (b) and the comparison of their sensor performance (c) The number inside (a) and (b) shows the load applied to the sensor.

In summary, both piezoelectrets can be used as pressure sensors. P1-4 sensor can cover broader pressure range but with a lower sensitivity, whereas the P2-3 sensor has a higher sensitivity but with reduced sensing range. Therefore, the piezoelectric pressure sensor could be customized to fulfill the different demands by changing the structure parameters in 3D printing, leading to a structure – performance design and implementation capability not achievable by other fabrication technologies. In addition, the structure demonstrated herein could be viewed as a sensing element that can be easily expanded to large areas by 3D printing, leading to sensor arrays and large area sensor for distributive sensing.

5. Conclusion

In summary, the study reports the successful fabrication of piezoelectrets with different piezoelectric sensitivity by direct 3D printing. The printing process overcame several distinct difficulties unique to the printing of porous structures without the use of support structure. By using different structural design in combination of design parameters, piezoelectrets with different piezoelectric activities can be printed. The sensing performance of the printed piezoelectrets were demonstrated using two prototype sensors. This study, for the first time, shows 3D printing has great potential as a general strategy for the fabrication of piezoelectrets with designed piezoelectric properties and sensor characteristics (sensitivity, sensing range, flexible vs. rigid), by rationale design of the piezoelectret architecture. Currently the two designs offered either high sensitivity with limited sensing range or a wide sensing range with reduced sensitivity. This limitation may be addressed in the future by optimizing the unit cell designs. For example, a design of mixed unit cells, *e.g.*, unit cells with the same basic geometry but with different dimensions, or unit cells with different geometries may be explored to expand the piezoelectrets sensor performance space.

Conflict of Interest

There is no conflict of interest.

Supporting Information

Applicable.

References

[1] J. Hillenbrand, G. M. Sessler, Piezoelectricity in cellular electret films, *IEEE Transactions on Dielectrics and Electrical Insulation*, 2000, **7**, 537-542, doi: 10.1109/94.868074.

[2] M. Wegener, S. Bauer, Microstorms in cellular polymers: a route to soft piezoelectric transducer materials with engineered macroscopic dipoles, *ChemPhysChem*, 2005, **6**, 1014-1025, doi: 10.1002/cphc.200400517.

[3] X. Zhang, J. Hillenbrand, G. M. Sessler, S. Haberzettl, K. Lou, Fluoroethylenepropylene ferroelectrets with patterned microstructure and high, thermally stable piezoelectricity, *Applied Physics A*, 2012, **107**, 621-629, doi: 10.1007/s00339-012-6840-7.

[4] R. Pisani Altafim, D. Rychkov, W. Wirges, R. Gerhard, H. Basso, R. Correa Altafim, M. Melzer, Laminated tubular-channel ferroelectret systems from low-density polyethylene films and from fluoroethylene- propylene copolymer films - A comparison, *IEEE Transactions on Dielectrics and Electrical Insulation*, 2012, **19**, 1116-1123, doi: 10.1109/tdei.2012.6259978.

[5] F. Peng, H. Lars, W. Werner, G. Reimund, Piezoelectric d33 coefficients in foamed and layered polymer piezoelectrets from dynamic mechano-electrical experiments, electro-mechanical resonance spectroscopy and acoustic-transducer measurements, *Measurement Science and Technology*, 2012, **23**, 035604, doi: 10.1088/0957-0233/23/3/035604.

[6] R. A. C. Altafim, H. C. Basso, R. A. P. Altafim, L. Lima, C. V. de Aquino, L. G. Neto, R. Gerhard-Multhaupt, Piezoelectrets from thermo-formed bubble structures of fluoropolymer-electret films, *IEEE Transactions on Dielectrics and Electrical Insulation*, 2006, **13**, 979-985, doi: 10.1109/tdei.2006.247822.

[7] Z. An, M. Mao, J. Cang, Y. Zhang, F. Zheng, significantly improved piezoelectric thermal stability of cellular polypropylene films by high pressure fluorination and post-treatments, *Journal of Applied Physics*, 2012, **111**, 024111, doi: 10.1063/1.3679576.

[8] X. Zhang, J. Hillenbrand, G. M. Sessler, Piezoelectric d33 coefficient of cellular polypropylene subjected to expansion by pressure treatment, *Applied Physics Letters*, 2004, **85**, 1226-1228, doi: 10.1063/1.1781388.

[9] R. H. Ali Samadi, T. Azdast, H. Abdollahi, P. Zarrintaj, M. R. Saeb, *Journal of Macromolecular Science: Part B*, 2020, **59**, 14, doi: 10.1080/00222348.2020.1730573.

[10] B. Gustavo Ortega, S. Pedro Llovera, M. Francisco, Q. Alfredo, *Journal of Physics: Conference Series*, 2011, **301**, 012054, doi: 10.1088/1742-6596/301/1/012054.

[11] M. Wegener, W. Wirges, J. Fohlmeister, B. Tiersch, R. Gerhard-Multhaupt, Two-step inflation of cellular polypropylene films: void-thickness increase and enhanced electromechanical properties, *Journal of Physics D: Applied Physics*, 2004, **37**, 623, doi: 10.1088/0022-3727/37/4/013.

[12] Y. Li, C. Zeng, Low-temperature CO2-assisted assembly of cyclic olefin copolymer ferroelectrets of high piezoelectricity and thermal stability, *Macromolecular Chemistry and Physics*, 2013, **214**, 2733-2738, doi: 10.1002/macp.201300440.

[13] H. Wang, Y. Li, X. Wang, Z. Liu, M. F. Ahmed, C. Zeng, Preparation and characterization of piezoelectric foams based on cyclic olefin copolymer, *Engineered Science*, 2021, **16**, 203-210, doi: 10.30919/es8d560.

[14] X. Zhang, J. Huang, X. Wang, Z. Xia, Piezoelectricity and dynamic characteristics of laminated fluorocarbon films, *IEEE Transactions on Dielectrics and Electrical Insulation*, 2010, **17**, 1001-1007, doi: 10.1109/tdei.2010.5539667.

[15] X. Zhang, X. Zhang, G. M. Sessler, X. Gong, Quasi-static and dynamic piezoelectric responses of layered polytetrafluoroethylene ferroelectrets, *Journal of Physics D: Applied Physics*, 2014, **47**, 015501, doi: 10.1088/0022-3727/47/1/015501.

[16] X. Zhang, J. Hillenbrand, G. M. Sessler, Thermally stable fluorocarbon ferroelectrets with high piezoelectric coefficient, *Applied Physics A*, 2006, **84**, 139-142, doi: 10.1007/s00339-006-3573-5.

[17] X. Zhang, G. Cao, Z. Sun, Z. Xia, Fabrication of fluoropolymer piezoelectrets by using rigid template: Structure and thermal stability, *Journal of Applied Physics*, 2010, **108**, 064113, doi: 10.1063/1.3482011.

[18] G. S. Neugschwandtner, R. Schwödiauer, S. Bauer-Gogonea, S. Bauer, Large piezoelectric effects in charged, heterogeneous fluoropolymer electrets, *Applied Physics A Materials Science & Processing*, 2000, **70**, 1-4, doi: 10.1007/pl00006965.

[19] X. Zhang, X. Wang, G. Cao, D. Pan, Z. Xia, Polytetrafluoroethylene piezoelectrets prepared by sintering process, *Applied Physics A*, 2009, **97**, 859-862, doi: 10.1007/s00339-009-5341-9.

[20] R. Gerhard-Multhaupt, W. Kunstler, T. Gome, A. Pucher, T. Weinhold, M. Seiss, Z. Xia, A. Wedel, R. Danz, Porous PTFE space-charge electrets for piezoelectric applications, *IEEE Transactions on Dielectrics and Electrical Insulation*, 2000, **7**, 480-488, doi: 10.1109/94.868065.

[21] A. Alderson, K. L. Alderson, S. A. McDonald, B. Mottershead, S. Nazare, P. J. Withers, Y. T. Yao, Piezomorphic materials, *Macromolecular Materials and Engineering*, 2013, **298**, 318-327, doi: 10.1002/mame.201200028.

[22] J. Hillenbrand, G. M. Sessler, High-sensitivity piezoelectric microphones based on stacked cellular polymer films (L), *The Journal of the Acoustical Society of America*, 2004, **116**, 3267-

3270, doi: 10.1121/1.1810272.
[23] M. Wegener, E. Tuncer, W. Wirges, R. Gerhard-Multhaupt, M. Dansachmuller, S. Bauer-Gogonea, R. Schwodiauer, S. Bauer, Ferroelectrets: highly anisotropic electrically charged polymer foams for electromechanical transducer applications, *IEEE Ultrasonics Symposium*, 2004, **2**, 1138-1141, doi: 10.1109/ultsym.2004.1417981
[24] Y. Feng, K. Hagiwara, Y. Iguchi, Y. Suzuki, Trench-filled cellular parylene electret for piezoelectric transducer, *Applied Physics Letters*, 2012, **100**, 262901, doi: 10.1063/1.4730952.
[25] J. Hillenbrand, M. Kodejska, Y. Garcin, H. Seggern, G. Sessler, High-sensitivity piezoelectret-film accelerometers, *IEEE Transactions on Dielectrics and Electrical Insulation*, 2010, **17**, 1021-1027, doi: 10.1109/tdei.2010.5539670.
[26] P. Pondrom, J. Hillenbrand, G. M. Sessler, J. Bos, T. Melz, Energy harvesting with single-layer and stacked piezoelectret films, *IEEE Transactions on Dielectrics and Electrical Insulation*, 2015, **22**, 1470-1476, doi: 10.1109/tdei.2015.7116339.
[27] X. Zhang, G. M. Sessler, Y. Wang, Fluoroethylenepropylene ferroelectret films with cross-tunnel structure for piezoelectric transducers and micro energy harvesters, *Journal of Applied Physics*, 2014, **116**, 074109, doi: 10.1063/1.4893367.
[28] S. C. Stanton, A. Erturk, B. P. Mann, E. H. Dowell, D. J. Inman, Nonlinear nonconservative behavior and modeling of piezoelectric energy harvesters including proof mass effects, *Journal of Intelligent Material Systems and Structures*, 2012, **23**, 183-199, doi: 10.1177/1045389x11432656.
[29] L. J. Gibson, M. F. Ashby, Cellular solids: structure and properties, Cambridge University Press, 1997, ISBN:131602542X, doi: 10.1017/cbo9781139878326.
[30] W. S. Boyle, P. Kisliuk, Departure from paschen's law of breakdown in gases, *Physical Review*, 1955, **97**, 255-259, doi: 10.1103/PhysRev.97.255.
[31] F. Peng, Q. Xunlin, W. Wirges, R. Gerhard, L. Zirkel, Polyethylene-naphthalate (PEN) ferroelectrets: cellular structure, piezoelectricity and thermal stability, *IEEE Transactions on Dielectrics and Electrical Insulation*, 2010, **17**, 1079-1087, doi: 10.1109/TDEI.2010.5539678
[32] M. Wegener, W. Wirges, R. Gerhard-Multhaupt, M. Dansachmüller, R. Schwödiauer, S. Bauer-Gogonea, S. Bauer, M. Paajanen, H. Minkkinen, J. Raukola, Controlled inflation of voids in cellular polymer ferroelectrets: Optimizing electromechanical transducer properties, *Applied Physics Letters*, 2004, **84**, 392-394, doi: 10.1063/1.1641171.
[33] A. Kachroudi, S. Basrour, L. Rufer, A. Sylvestre, F. Jomni, Dielectric properties modelling of cellular structures with PDMS for micro-sensor applications, *Smart Materials and Structures*, 2015, **24**, 125013, doi: 10.1088/0964-1726/24/12/125013.
[34] H.-J. Yen, C.-S. Tseng, S.-H. Hsu, C.-L. Tsai, Evaluation of chondrocyte growth in the highly porous scaffolds made by fused deposition manufacturing (FDM) filled with type II collagen, *Biomedical Microdevices*, 2009, **11**, 615-624, doi: 10.1007/s10544-008-9271-7.
[35] H. N. Chia, B. M. Wu, Recent advances in 3D printing of biomaterials, *Journal of Biological Engineering*, 2015, **9**, 4, doi: 10.1186/s13036-015-0001-4.
[36] I. Zein, D. W. Hutmacher, K. C. Tan, S. H. Teoh, Fused deposition modeling of novel scaffold architectures for tissue engineering applications, *Biomaterials*, 2002, **23**, 1169-1185, doi: 10.1016/s0142-9612(01)00232-0.
[37] F. Wang, L. Shor, A. Darling, S. Khalil, W. Sun, S. Güçeri, A. Lau, Precision extruding deposition and characterization of cellular poly-ε-caprolactone tissue scaffolds, *Rapid Prototyping Journal*, 2004, **10**, 42-49, doi: 10.1108/13552540410512525.
[38] F. Bos, R. Wolfs, Z. Ahmed, T. Salet, Additive manufacturing of concrete in construction: potentials and challenges of 3D concrete printing, *Virtual and Physical Prototyping*, 2016, **11**, 209-225, doi: 10.1080/17452759.2016.1209867.
[39] S. J. Kalita, S. Bose, H. L. Hosick, A. Bandyopadhyay, Development of controlled porosity polymer-ceramic composite scaffolds via fused deposition modeling, *Materials Science and Engineering: C*, 2003, **23**, 611-620, doi: 10.1016/s0928-4931(03)00052-3.
[40] D. Drummer, S. Cifuentes-Cuéllar, D. Rietzel, Suitability of PLA/TCP for fused deposition modeling, *Rapid Prototyping Journal*, 2012, **18**, 500-507, doi: 10.1108/13552541211272045.
[41] Z. Liu, M. Zeng, H. Wang, X. Wang, Y. Li, C. Zeng, Toward flexible piezoelectrets with high environmental stability: a hybrid approach, *ES Materials & Manufacturing*, 2022, **17**, 73-82, doi: 10.30919/esmm5f631.
[42] A. Haleem, V. Kumar, L. Kumar, Mathematical modelling & pressure drop analysis of fused deposition modelling feed wire, *International Journal of Engineering and Technology*, 2017, **9**, 2885-2894, doi: 10.21817/ijet/2017/v9i4/170904066.

Author Information

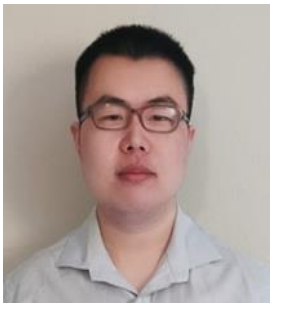

Xiaolin Wang *received his B.S degree in polymer science and engineering from Sichuan university in China and master's degree in material science in Washington state university. He is currently a Ph.D. candidate in Department of Industrial & Manufacturing Engineering at Florida State University. Xiaolin Wang's research focus on the design and fabrication of the piezoelectrets with 3D printing technology.*

Dr. Hui Wang *received his Ph.D. degree in Industrial Engineering from Florida State University. His research interest is piezoelectric materials and its applications & engineering statistical models.*

Dr. Zhe Liu *is a Materials and Process Engineer at Maxar technologies. Prior to joining in Maxar, she worked at Arevo. Inc. to develop the materials and process for continuous carbon fiber composite manufacturing. She earned her Ph. D. from Florida State University with a focus on the composite and smart materials design, manufacturing, characterization and simulation.*

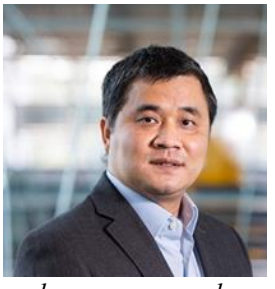

Dr. Changchun Zeng *is Professor and Chair of the Department of Industrial & Manufacturing Engineering. Dr. Zeng's research is in the areas of innovative materials and advanced manufacturing technology, particularly in multifunctional polymeric materials and porous polymeric materials, and their novel manufacturing process and applications in industrial and biomedical fields. He has published extensively and hold multiple patents in these areas. Professor Zeng is a recipient of Florida State University's Developing Scholar Award, and the Research Excellence Award from FSU College of Engineering. He also serves as editor of Journal of Cellular Plastics. Professor Zeng received his PhD from The Ohio State University in 2004.*

